



# *Rubus fruticosus* leaf extract inhibits vascular dementia-induced memory impairment and neuronal loss by attenuating neuroinflammation

Nak Song Sung<sup>1\*</sup>, Sun Ho Uhm<sup>2\*</sup>, Hyun Bae Kang<sup>2\*</sup>, Nam Seob Lee<sup>3</sup>, Young-Gil Jeong<sup>3</sup>, Do Kyung Kim<sup>3</sup>, Nak-Yun Sung<sup>4</sup>, Dong-Sub Kim<sup>4</sup>, Young Choon Yoo<sup>5</sup>, Seung Yun Han<sup>3</sup>


<sup>1</sup>Department of General Surgery, Konyang University Hospital, Daejeon, <sup>2</sup>Research Institute, Healnols Inc., Daejeon, <sup>3</sup>Department of Anatomy, College of Medicine, Konyang University, Daejeon, <sup>4</sup>Division of Natural Product Research, Korea Prime Pharmacy Co., Ltd., Gwangju, <sup>5</sup>Department of Microbiology, College of Medicine, Konyang University, Daejeon, Korea

**Abstract:** Vascular dementia (VaD) is characterized by progressive memory impairment, which is associated with microglia-mediated neuroinflammation. Polyphenol-rich natural plants, which possess anti-inflammatory activities, have attracted scientific interest worldwide. This study investigated whether *Rubus fruticosus* leaf extract (RFLE) can attenuate VaD. Sprague–Dawley rats were separated into five groups: SO, sham-operated and treated with vehicle; OP, operated and treated with vehicle; RFLE-L, operated and treated with low dose (30 mg/kg) of RFLE; RFLE-M, operated and treated with medium dose (60 mg/kg) of RFLE; and RFLE-H, operated and treated with high dose (90 mg/kg) of RFLE. Bilateral common carotid artery and hypotension were used as a modeling procedure, and the RFLE were intraorally administered for 5 days (preoperative 2 and postoperative 3 days). The rats then underwent memory tests including the novel object recognition, Y-maze, Barnes maze, and passive avoidance tests, and neuronal viability and neuroinflammation were quantified in their hippocampi. The results showed that the OP group exhibited VaD-associated memory deficits, neuronal death, and microglial activation in hippocampi, while the RFLE-treated groups showed significant attenuation in all above parameters. Next, using BV-2 microglial cells challenged with lipopolysaccharide (LPS), we evaluated the effects of RFLE in dynamics of proinflammatory mediators and the upstream signaling pathway. RFLE pretreatment significantly inhibited the LPS-induced release of nitric oxide, TNF- $\alpha$ , and IL-6 and upregulation of the MAPKs/NF- $\kappa$ B/iNOS pathway. Collectively, we suggest that RFLE can attenuate the histologic alterations and memory deficits accompanied by VaD, and these roles are, partly due to the attenuation of microglial activation.

**Key words:** Vascular dementia, *Rubus fruticosus*, Microglia, Neuroinflammation, Memory deficit

Received July 16, 2023; Revised July 24, 2023; Accepted July 25, 2023

## Corresponding author:

Seung Yun Han   
Department of Anatomy, College of Medicine, Konyang University,  
Daejeon 35365, Korea  
E-mail: jjzy@konyang.ac.kr

\*These authors contributed equally to this work.

## Introduction

Vascular dementia (VaD) is a neurodegenerative disorder that induces memory impairment and is caused by a vascular obstruction in the brain. VaD accounts for approximately 18%–20% of all dementia cases in elderly people and is the second most common subtype of dementia following Al-

Copyright © 2023. Anatomy & Cell Biology

This is an Open Access article distributed under the terms of the Creative Commons Attribution Non-Commercial License (<http://creativecommons.org/licenses/by-nc/4.0/>) which permits unrestricted non-commercial use, distribution, and reproduction in any medium, provided the original work is properly cited.

zheimer's disease (AD) [1]. The most important pathology induced by vascular obstruction is cerebral ischemia, which occurs in a discrete brain region that causes a significant decrease in cerebral blood flow (CBF) [2]. Upon deprivation of oxygen and nutrients due to the decrease in CBF, ischemic neurons become susceptible to reactive oxygen species-associated oxidative stress and subsequent apoptosis, which in turn mediates neuroinflammation in adjacent brain areas [3]. Experimental evidence regarding the role of neuroinflammation in VaD explains that the "naïve" microglia in the responsible region might convert to "activated" microglia [4]. The resulting phosphorylation-dependent activation of mitogen-activated protein kinase (p38 MAPK), extracellular signal-regulated kinase (ERK) 1/2, c-Jun N-terminal kinase (JNK), inducible nitric oxide synthase (iNOS), together with nuclear translocation of nuclear factor kappa B (NF- $\kappa$ B) leads to the release of pro-inflammatory mediators, including nitric oxide (NO), tissue necrosis factor (TNF)- $\alpha$ , and interleukin (IL)-6 [4, 5]. These events are aggravated by a breakdown of the blood-brain barrier, which enhances the extravasation of proinflammatory mediators [4-6]. All aforementioned events eventually result in neuronal death of the responsible regions, including the hippocampus, which is believed to be a key center of cognitive and memory functions [7].

Given the key roles of oxidative stress and neuroinflammation in VaD, screening of edible agents with antioxidant and anti-inflammatory properties has been of great interest [8]. Polyphenolic compounds, which are abundant in medicinal plants, are known to possess a wide range of biological effects, such as antibacterial [9, 10], antiviral [11], anti-aging [12], anti-cancer [13], antioxidative [14], and anti-inflammatory effects [15]. Among the polyphenol-rich medicinal plants, *Rubus fruticosus* (Rosaceae) or blackberries grow wild in most European countries, where their fruits have been used as a valuable source of dietary antioxidants because of their zesty flavor and high content of polyphenols [16, 17]. Apart from the fruits, their leaves are consumed as a form of traditional medicine for their astringent [18], antipyretic [19], and hypoglycemic activities [20]. Previous phytochemical investigations, which were carried out on *R. fruticosus* leaf extract (RFLE), have proved the presence of bioactive single compounds such as flavonoids, ellagic acid (EA), and tannins [21].

However, excluding the Riaz et al.'s [22] report regarding the antidepressant activity of RFLE on depression, there is

an absolute dearth of reports concerning central nervous system (CNS) diseases including VaD. To address this gap, we prepared the ethanolic extract of RFLE (hereinafter, simply referred as RFLE) and determined whether RFLE consumption could attenuate VaD. To do this, we evaluated the therapeutic efficacy of RFLE in an VaD model *in vivo* and investigated the underlying mechanism focusing on microglial activation using a murine microglial cell line *in vitro*.

## Materials and Methods

### Preparation of RFLE

RFLE was kindly supplied by the Korea Prime Pharm Co., Ltd. in August 2022. Hot air drying was performed at 50°C in a drying oven (PURIVEN 150; Cryste). Two kilograms of dried and crushed leaves were extracted in 50% ethanol with reflux condensation at 85°C for 4 hours. Undissolved residues were discarded by filtration with a filter paper (No. 42; Whatman). The filtrate was evaporated under vacuum using a rotary evaporator (EYELA N-3010) at 40°C, and the residue was lyophilized using a freeze dryer (FD 8508; IL-ShinBioBase). The dried ethanolic extracts, 615 g; extraction yield, 30.8%) were stored at 4°C until their use.

### High performance liquid chromatography (HPLC)

An LC-20AD HPLC system using an SPD-M20A diode array detector and Phenomenex Gemini NX-C18 column (4.6×250 mm, 5  $\mu$ m; Shimadzu) was employed to confirm the existence of EA in RFLE, as reported in a previous study [21]. The mobile phase consisted of two parts (solvents A and B). Solvent A was 0.5% phosphoric acid in the water, and solvent B was 0.1% phosphoric acid in acetonitrile. The gradient was 0–5 minutes, 5%–15% B; 5–25 minutes, 15%–20% B; 25–35 minutes, 20%–100% B; 35–40 minutes, 100% B; 40–41 minutes, 5%–100% B; and 41–50 minutes, 5% B (a run time, 50 min; a flow rate, 1.0 ml/min). The phenolic constituents were analyzed by the retention time and UV-visible spectra of the EA standard measured from the peak at 254 nm. Peaks were identified by comparing their relative retention times with those of the EA standard and analyzed under the same conditions as presented in Fig. 1.

### Animals

A total of 50 Sprague–Dawley rats (9 weeks old, male, 250–300 g) were purchased from Samtako. They were stabilized in an environmentally static room for 7 days at a con-

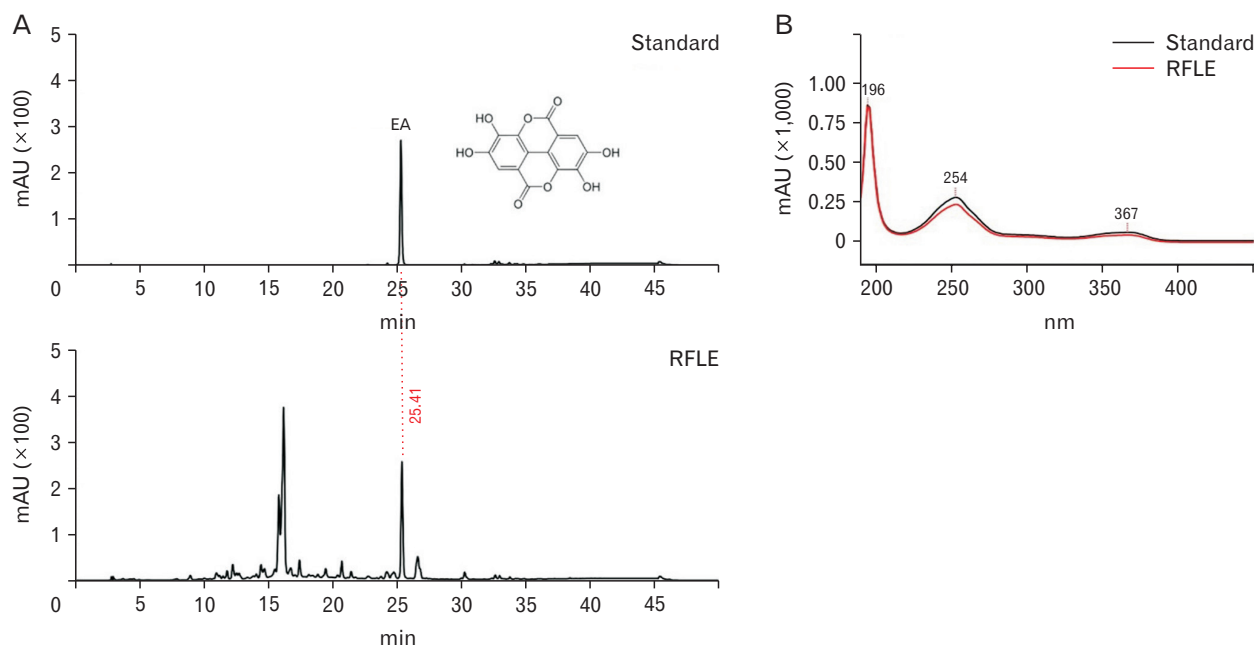


**Fig. 1.** HPLC chromatograms of standard ellagic acid (EA) and RFLE obtained using a NX-C18 column (Shimadzu) monitored at 254 nm of peak area, 50 minutes of run time, and 1.0 ml/min-of flow rate. (A) The retention time for standard EA was compared with the chromatogram of RFLE, which showed sharp peaks generated at the same time point (25.41 min). (B) The UV-visible spectra of the extract corresponding to the standard EA peak. HPLC, high performance liquid chromatography; RFLE, *Rubus fruticosus* leaf extract.

trolled temperature (21°C–23°C) and humidity (43%–63%) under a 12 hours light/dark cycle. Water and food were provided *ad libitum*. Rats were housed in groups of five per cage and randomly assigned to different groups for all experiments. The experiments were performed in accordance with the Guide for the Care and Use of Laboratory Animals (National Institutes of Health publication, 8th Edition, 2012) [23]. The *in vivo* experiments were approved by the Konyang Institutional Animal Care and Use Committee (IACUC; #P-22-31-A-15).

### Experimental plan

All animals were randomly divided into four groups and given differently as follows: a vehicle (distilled water; n=20), a low dose of RFLE (30 mg/kg [RFLE-L]; n=10), a medium dose of RFLE (60 mg/kg [RFLE-M]; n=10), and a high dose of RFLE (90 mg/kg [RFLE-H]; n=10). The RFLE was diluted in a vehicle to yield a volume of 1 ml and administered introrally once a day for a total of 5 days (2 days before operation, the day of operation, and 2 days after operation). The selection of a high dose of RFLE was based on dose conversion protocols, as described previously [24]. Just prior to the operation, the groups with vehicles were further assigned to

two subgroups (n=10/group): subjected to sham operation (SO) and operation (OP), eventually yielding five groups titled “SO,” “OP,” “RFLE-L,” “RFLE-M,” and “RFLE-H.” On postoperative day (POD) 3, all groups underwent four different behavioral tests, *i.e.*, novel object recognition test (NORT), Barnes maze test (BMT), Y-maze test (Y-MT), and passive avoidance test (PAT), in sequential order. After completing all tests, the rats were sacrificed for brain sampling, followed by histological analyses. The time flow of the *in vivo* experiments is shown in Fig. 2A.

### Bilateral common carotid artery occlusion and hypotension

Bilateral common carotid artery occlusion and hypotension (BCCAO/H) were used to establish a rat model of VaD according to a previously described method, as schematically illustrated in Fig. 2B [25, 26]. In brief, the rats were anesthetized with 3% isoflurane in a gas mixture (70% N<sub>2</sub>O and 30% O<sub>2</sub>), and anesthesia was maintained throughout the operation at a level of 1%–3% isoflurane. The core temperature was maintained at 37°C using a heating pad during the entire operation. Prior to the neck approach, the left femoral artery was catheterized with a PE-50 catheter coupled with a

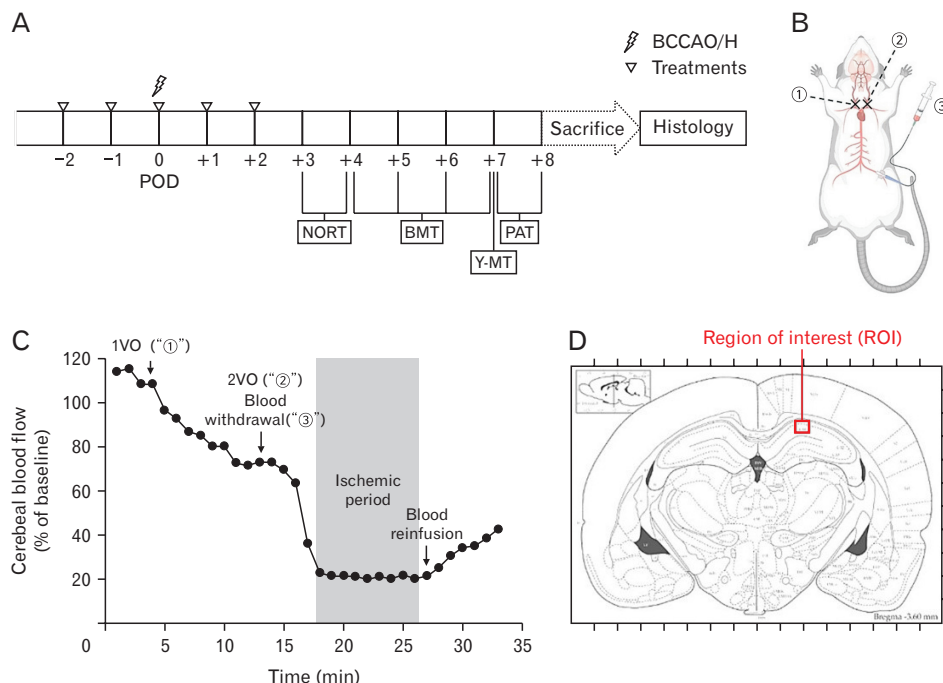


**Fig. 2.** Graphical illustration of the *in vivo* experiment. (A) Schematic schedule, (B) operation procedure, (C) a representative Doppler flowmetry during the operation, and (D) region of interest for histologic studies are presented. In (B), circled “1”, “2”, and “3” represent the steps of right common carotid artery ligation, left common carotid artery ligation, and blood withdrawal via a femoral artery catheter, respectively, during BCCAO/H operation. In (D), the red box (300 μm in width) in hippocampal cornu ammonis 1 point out a region of interest for histologic analyses. POD, postoperative day; BCCAO/H, bilateral common carotid artery occlusion and hypotension; NORT, novel object recognition test; BMT, Barnes maze test; Y-MT, Y-maze test; PAT, passive avoidance test; VO, vessel occlusion.

syringe to permit future withdrawal of blood. After the mid-line neck incision, the right and left common carotid arteries were exposed and transiently occluded with aneurysmal clips, one after the other. Next, blood was withdrawn via the catheterized femoral artery at a constant speed (3 ml/min) to cause systemic hypotension. When the relative CBF (rCBF) reached below 20% of the baseline, as monitored by Periflux 5000 Doppler flowmeter (Perimed AB), the blood withdrawal was stopped and an 8 minutes ischemic period was started (Fig. 2C). At this period, blood in a syringe was kept in a homeothermic bath set at 37°C to prevent clotting. At the end of the ischemic period, the clips on both common carotid arteries were removed, and blood was reinfused at a constant speed (3 ml/min) via a femoral catheter. After confirming a gradual rise in rCBF, all surgical wounds were closed and the rats were returned to their home cages.

**Novel object recognition test**

The NORT was employed to assess the recognition memory performance of the rats. During the familiarization session, each individual rat was introduced to the center of a matte black square box of size 70×70×35 cm containing two identical objects spaced diagonally at 30-cm intervals. The rat was allowed to freely explore the objects for 10 minutes. After 24 hours, the rat underwent the test session, at which point one of the familiar objects was replaced by a novel ob-

ject. The rats were allowed to freely explore the objects for 10 minutes. The positivity of object preference was judged by a rat directing its nose to within 2 cm of the object, touching it, rearing on it, or staying beside it for over 5 seconds. The exploratory behavior of individual rats during the familiarization and test sessions was analyzed with the aid of a video tracking system (EthoVision XT9; Noldus), and averaged for each group. After each rat was tested, the box and objects were cleaned with 70% ethanol.

**Barnes maze test**

The BMT was used to assess the spatial learning and memory performance of the rats. For this, a 122-cm diameter and 100-cm high circular maze was utilized. Among the twenty holes in the peripheral location, one of these was installed on an escape box (20×15×12 cm). Each individual rat was placed on a table and given 300 seconds to enter the escape box under illumination as aversive stimuli. For 4 days, each animal performed one trial per day. During the trial session, the latency(s) to escape the platform and trajectory of the rats were recorded with the aid of a video tracking system (EthoVision XT9) and averaged for each group. If the rat failed to enter the escape platform in 300 seconds, 300 seconds was given as the record. After each trial, the apparatus was cleaned with 70% ethanol.

### ***Y-maze test***

The Y-MT was used as a second tool to assess the spatial learning and memory performance of the rats. Each individual rat was introduced to the center of a matte black plastic maze with three arms (50 cm in length, 15 cm in width, and 30 cm in height) spaced at 120° intervals. The total number and entering sequences were traced for a period of 8 minutes. The number of total arm entries was also measured as an indicator of locomotor activity. The percentage of spontaneous alternation was calculated according to the following formula: spontaneous alternation (%) = [(number of alternations)/(total arm entries - 2)] × 100 [26].

### ***Passive avoidance test***

The PAT was performed to assess the contextual fear memory of the rats. The apparatus was divided into two chambers: an illuminated and a dark chamber, each measuring 25 cm in length, 20 cm in width, and 25 cm in height. The illuminated chamber was equipped with a lamp (50 W) which was used as an aversive stimulus. Each test consisted of two separate sessions, that are a trial session and a test session. During the trial session, each individual rat was initially introduced to the illuminated chamber. Once the rat moved to the dark chamber, the “trial latency” was recorded using a stopwatch. The measurements were triplicated, and an electric shock (0.5 mA, 3 sec) was given using stainless steel rods at the last entry into the dark chamber. After 24 hours, a test session was started. In this session, the “escape latency” to enter the dark chamber from the illuminated chamber was traced (<300 sec) and averaged for each group [26].

### ***Tissue processing and cresyl violet staining***

After completion of the memory function tests, the rats were anesthetized with an intraperitoneal administration of 100 mg/kg thiopental (Nycomed), and the brains were removed after transcardial perfusion with 4% paraformaldehyde (PFA) diluted in phosphate-buffered saline (PBS). The isolated brains were postfixed in 4% PFA, dehydrated, embedded in paraffin wax, and sectioned at 5-μm thickness using a tissue microtome (RM2255; Leica). In each rat, randomly selected two slides from the hippocampus-bearing tissues (-3.5 to -4.5 mm from the bregma in the anteroposterior axis) were deparaffinized and hydrated. After washing in PBS, the tissues were immersed in a cresyl violet (C-V) solution (0.1%; Abcam). The hippocampal cornu ammonis

1 (CA1) were captured using a digital camera connected to a DM4 light microscope (Leica; 400×). From the images, the number of healthy neurons characterized with clear nuclei and large soma in the region of interest (ROI; CA1 area sized to 300 μm in width; depicted red rectangular box in Fig. 2D) was counted and averaged for each group.

### ***Immunohistochemistry***

The other two slides randomly chosen from each rat were deparaffinized and incubated with rabbit antibody against ionized calcium-binding adapter molecule 1 (Iba1; Abcam) diluted in PBS (1:200) for 24 hours at 4°C in a humid chamber. After washing in PBS, each slide was incubated with biotinylated anti-rabbit IgG antibody diluted in PBS (1:250) for 2 hours at 23°C in a humid chamber. After washing in PBS, the slides were furtherly incubated with an avidin-biotin complex (VECTASTAIN<sup>™</sup> ABC Kits; Vector Laboratories Inc.), which was diluted in PBS (1:250) for 1 hour at 23°C. The resulting brown-colored immunoreactivities were obtained after the addition of 3,3'-diaminobenzidine (Vector Laboratories Inc.), a chromogen. After mounting, the ROI (depicted in Fig. 2D) was photographed using a digital camera connected to a DM4 light microscope (400×). In each ROI, the number of Iba1-immunopositive (Iba1<sup>+</sup>) cells was counted manually. The results were averaged per group.

### ***Cell culture and cell viability assay***

BV-2 cells (American Type Culture Collection), a murine microglial cell line, were maintained in Dulbecco's Modified Eagle Medium supplemented with 10% fetal bovine serum and 1% penicillin/streptomycin in a CO<sub>2</sub> incubator maintained at 37°C. To determine the appropriate dosage of RFLC treatment, the cells were seeded in a 96-well culture plate (1 × 10<sup>4</sup> cells per well) and kept for 24 hours at 37°C. The cells were then treated with RFLC (0–200 μg/ml) for 6 hours and further stimulated with or without lipopolysaccharide (LPS; 1 μg/ml) for 18 hours. The 3-(4,5-dimethylthiazol-2-yl)-2,5-diphenyl tetrazolium bromide (MTT) assays were utilized to assess cell viability in accordance with a previous study [25]. The MTT solution, which was created by diluting MTT in PBS to a final concentration of 0.5 mg/ml, was reacted with the cells for 4 hours at 37°C. After the reaction, the resulting insoluble formazan crystals in the bottom were diluted in 100 μl dimethyl sulfoxide. The absorbance was measured at 540 nm in a microplate reader (ELx800UV; BioTek). The resulting data were represented as % of untreated control.

### Measurement of NO and cytokines

Cells ( $5 \times 10^4$  cells/well) were pretreated with RFLE (0–200  $\mu\text{g/ml}$ ) for 6 hours and stimulated with 1  $\mu\text{g/ml}$  LPS for an additional 18 hours. Then, 100  $\mu\text{l}$  of the culture medium was collected and reacted with different reagents supplied by the NO, TNF- $\alpha$ , and IL-6 ELISA kits, according to the supplier's manual (R&D Systems) in accordance with a previous study [26]. The resulting absorbance was measured with an ELX-800UV microplate reader at 540 nm and each content was quantitatively measured by comparison with the standard curve.

### Western blot

Cells in 12-well culture plates ( $1 \times 10^7$  cells/well) were pretreated with RFLE (0–200  $\mu\text{g/ml}$ ) for 6 hours and stimulated with 1  $\mu\text{g/ml}$  LPS for an additional 18 hours. The cell pellets obtained by centrifuge were resuspended in lysis buffer (PRO-PREP<sup>TM</sup>; iNtRON) and furtherly centrifuged. Protein concentrations in the supernatant were determined using a bicinchoninic acid assay kit (QuantiPro<sup>TM</sup>; Sigma). A protein sample was transferred from a sodium dodecyl sulfate-polyacrylamide gel electrophoresis gel onto a polyvinylidene fluoride membrane (Bio-Rad) by electroblotting. The membranes were then incubated with primary antibodies including p38, phosphorylated (p-) p38, ERK, p-ERK, JNK, p-JNK, and iNOS, diluted in 5% skim milk solution (1:1,000). For blotting of NF- $\kappa\text{B}$ , a protein sample of the nuclear fraction was obtained using a cell compartment kit (Qproteome; QIAGEN).  $\beta$ -actin and laminB1 were used as loading controls for the total cell homogenate and nuclear fractions, respectively. After washing in PBS containing 0.1% Tween-20, the membrane was incubated with the horseradish peroxidase-conjugated secondary antibody diluted in 5% skim milk solution (1:1,000) for 1 hour, and the resulting bands were visualized using an enhanced chemiluminescence kit (Immobilon<sup>TM</sup>; Merck). All primary and secondary antibodies were purchased from Abcam. The band intensity was measured using ImageJ (v1.49, National Institutes of Health) and expressed as the relative intensity to that of  $\beta$ -actin or laminB1. All experiments were performed in triplicate.

### Statistical analyses

All data are presented as mean  $\pm$  standard error of the mean (SEM). Student's *t*-test, One-way ANOVA with Bonferroni *post-hoc* test for multiple comparisons were performed to determine the significant difference between different

groups (version 18; SPSS Inc.). *P*-values below 0.05 were considered statistically significant.

## Results

### RFLE attenuates memory impairment in a VaD rat

First, we performed HPLC to assess the quality of RFLE and confirm the presence of EA as the one of major component of RFLE. As shown in Fig. 1, one of the two major peaks was demonstrated to be EA. In standard references, EA appeared at 25.41 minutes and our results were consistent with previous results [17, 21]. Next, we investigated whether RFLE can attenuate the memory deficit using VaD rat model *in vivo*. As presented in the schematic overview of the *in vivo* experiment (Fig. 2A), we assessed the effects of 5 days (preoperative 2 and postoperative 3 days) of RFLE intake on the memory performance of the VaD rats. As shown in Fig. 2B, C, VaD rats were reliably produced by BCCAO/H operation under the guidance of Doppler flowmetry. From POD 3, the rats were subjected to four different memory tests, namely, NORT, BMT, Y-MT, and PAT, in a sequential manner. The NORT results demonstrated that all groups spent similar amounts of time exploring two identical objects (Fig. 3A) during the familiarization session. In the test session, while the SO group spent significantly more time exploring the new object than the familiar one (Fig. 3B,  $P < 0.001$ ), the OP group lacked this tendency. However, the RFLE-L, -M, and -H groups explored the new object for a significantly longer time than the familiar one ( $P < 0.05$ ,  $P < 0.001$ ), suggesting that the VaD-associated recognition memory deficit was reversed by RFLE (30 mg/kg or higher). Next, BMT was employed to assess the spatial learning and memory functions of the rats. The results showed that the majority of the rats failed to escape at the first trial, and thus the escape latencies of all groups were recorded as approximately 300 seconds (Fig. 3C). However, as more trials were conducted, the SO group spent less time finding the escape platform. The escape latency of the OP group was significantly longer than that of the SO group on the 4th day of the session ( $P < 0.01$ , Fig. 3C, D). The differences between the RFLE-L and OP groups were insignificant; however, the RFLE-M and -H groups showed a decrease in the escape latency on the 4th day of the session compared with that of the OP group ( $P < 0.05$ ,  $P < 0.01$ , respectively). In this test, neither the operation nor RFLE treatment significantly influenced motor performance, as tested by moving velocity (data not shown). Y-MT was adopted as

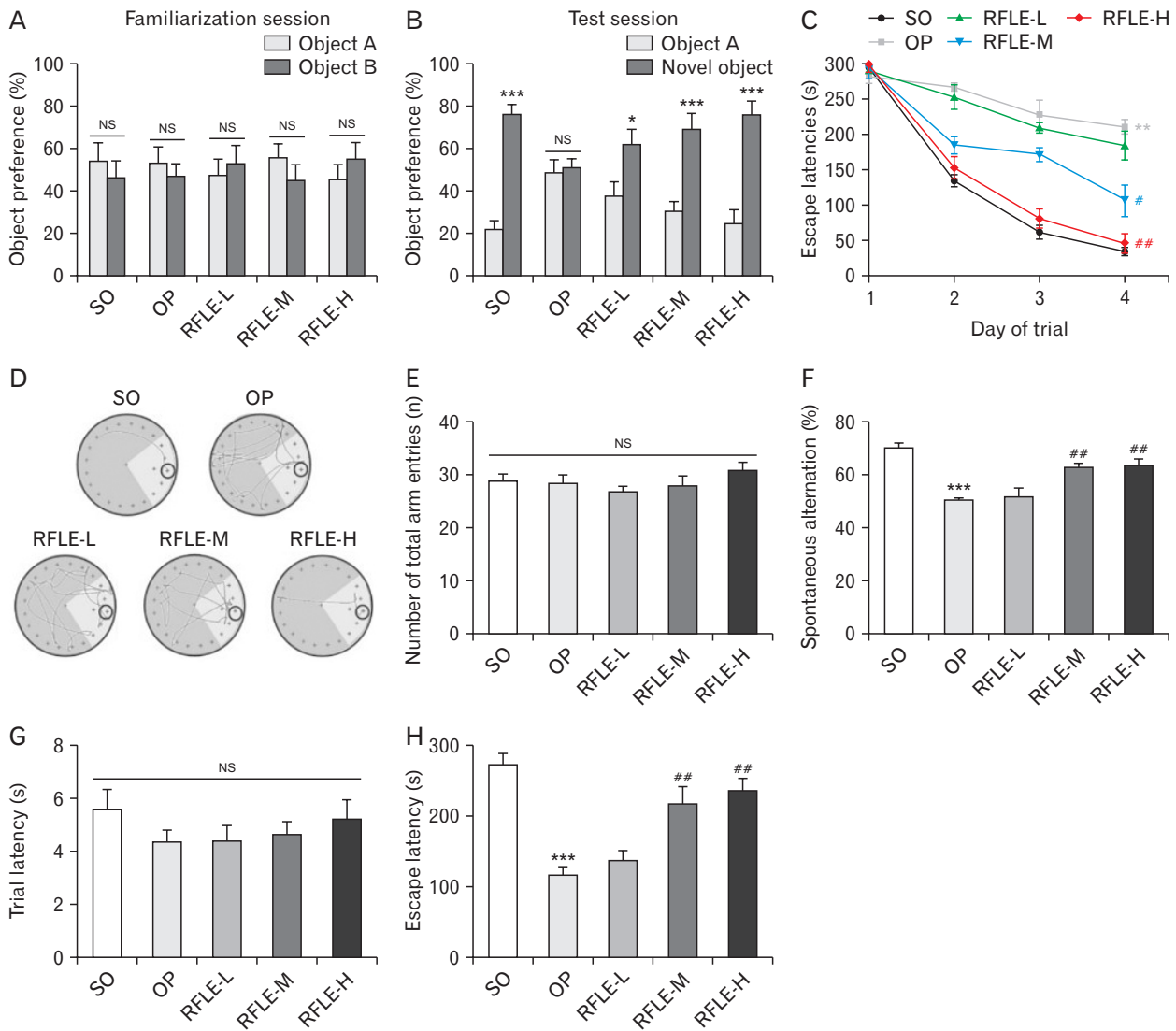


**Fig. 3.** Effects of RFLE on memory deficits in VaD rats. The percentage of time spent exploring (A) the two identical objects during the familiarization session and (B) the novel object over the familiar object during the test session under the novel object recognition test. (C) Time-dependent changes in escape latencies to the escape platform of different groups and (D) the representative tracking plots obtained at 4th trial day under the Barnes maze test. In tracking plots, the location of the escape platform is indicated as a black circle. (E) The number of total arm entries and (F) the percentage of spontaneous alternation of different groups were measured using the Y-maze test. (G) Trial latencies and (H) escape latencies of different groups were measured using the passive avoidance test. In all graphs, values are presented as mean±SEM (\**P*<0.05 and \*\*\**P*<0.001 vs. preference for familiar object in A and B; \*\**P*<0.01 and \*\*\**P*<0.001 vs. SO, #*P*<0.05 and ##*P*<0.01 vs. OP in the other graphs). RFLE, *Rubus fruticosus* leaf extract; VaD, vascular dementia; SO, sham operation; OP, operation; RFLE-L, operated and treated with low dose (30 mg/kg) of RFLE; RFLE-M, operated and treated with medium dose (60 mg/kg) of RFLE; RFLE-H, operated and treated with high dose (90 mg/kg) of RFLE; NS, not significant.

another tool for evaluating the spatial learning and memory functions of the rats. According to the Y-MT results, neither the operation nor RFLE treatment significantly influenced locomotor activity, as tested by the number of total arm entries (Fig. 3E). However, the OP group exhibited significant impairments in spatial memory, as observed by the reduction of spontaneous alternation (*P*<0.001 vs. SO; Fig. 3F). On the

contrary, the values were significantly spared in RFLE-M and -H groups when compared with the OP group (62.49±1.56 and 63.22±2.54 vs. 50.22±0.99, respectively; *P*<0.01), while the RFLE-L group showed no improvement. Finally, PAT was used to assess the contextual fear memory of the rats. Neither the operation nor RFLE treatment changed the trial latencies (Fig. 3G), however, the OP group developed a sig-

nificant memory impairment compared to the SO group, as demonstrated by the shorter escape latencies ( $P<0.001$ ; Fig. 3H) in the test sessions. Adversely, the latencies of the RFLE-M and -H groups were significantly longer than those of the OP group ( $215.50\pm 26.03$  and  $234.25\pm 19.26$  vs.  $115.50\pm 10.85$ , respectively;  $P<0.01$ ), while the RFLE-L group showed no improvement. Taken together, these results suggest that RFLE intake can attenuate memory impairment in VaD rats.

**RFLE attenuates VaD-associated deterioration in hippocampus**

Next, we investigated whether RFLE supplements could attenuate VaD-associated structural damage in the hippocampus, which has been known as an essential feature of VaD. Using C-V stain, the effects of perioperative RFLE treatment on the BCCAO/H-induced neuronal death in the

hippocampus, especially in the CA1 region. On POD 8, the OP group showed a marked decrease in the number of viable neurons located in the stratum pyramidale (SP) of hippocampal CA1 ( $P<0.001$  vs. SO; Fig. 4A, B). The OP group also showed the presence of apoptotic neurons showing shrunken cytoplasm and pyknotic nuclei in all three layers, *i.e.*, the stratum oriens, SP, and stratum radiatum. Remarkably, the number of viable neurons was significantly higher in the RFLE-L, -M, and -H groups than in the OP group ( $P<0.05$ ,  $P<0.01$ ), and this change was partially dose-dependent ( $P<0.05$  vs. RFLE-L). Since neuroinflammation and the key role of microglia in this process are known to be involved in VaD pathogenesis [27], we next quantified the population of microglia in the adjacent area by immunohistochemical detection of Iba1, a marker for microglia. The number of Iba1<sup>+</sup> microglia in the ROI was much higher in the OP group than

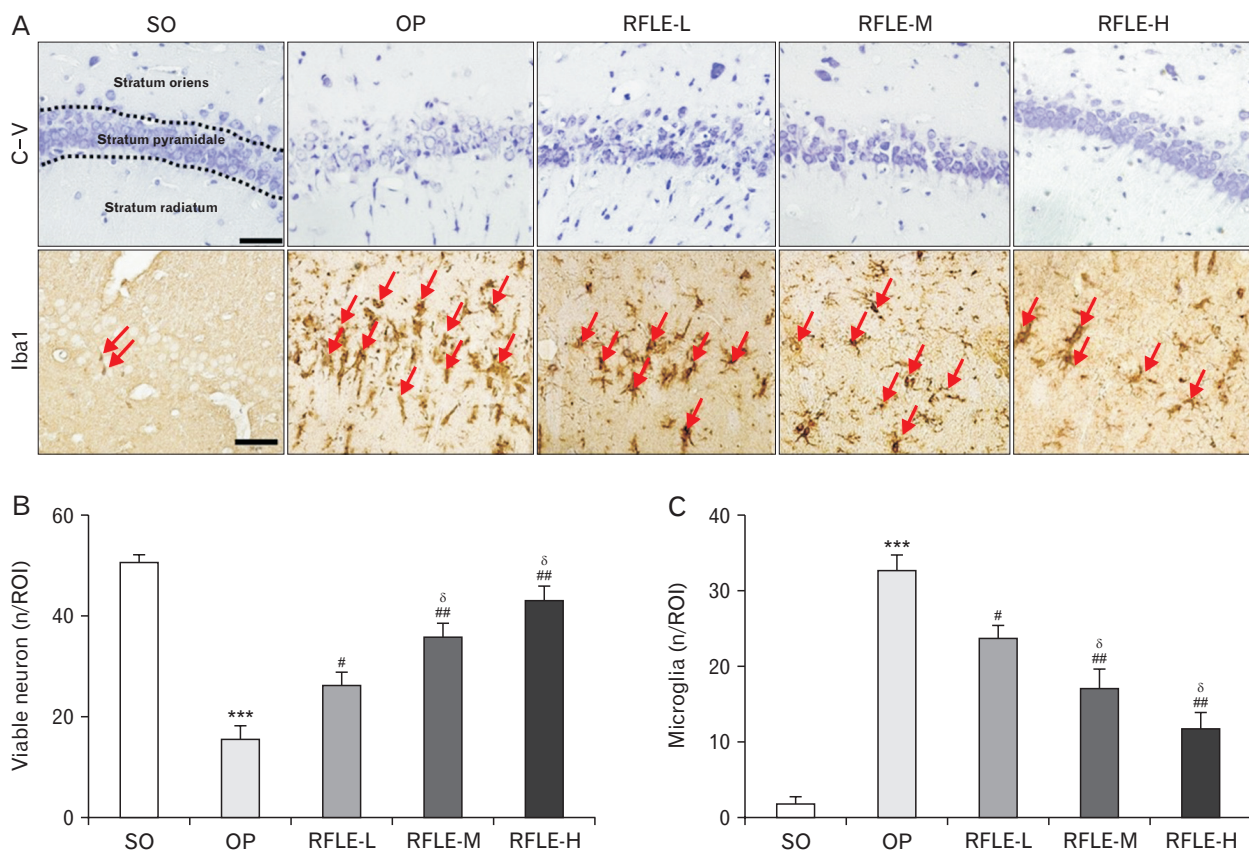


Fig. 4. Effects of RFLE on neuronal viability and microglial activation in hippocampal CA1 of the VaD rat. (A) Representative photographs of cresyl violet stained (top row) and Iba1-immunostained (bottom row) hippocampal CA1 tissues. Iba1-immunopositive microglia are indicated with red arrows. Scale bar=50 μm. (B) Quantitative graphs showing the number of viable pyramidal neurons and (C) microglia. In graphs, values are presented as mean±SEM (\*\*\*) $P<0.001$  vs. SO; # $P<0.05$  and ## $P<0.01$  vs. OP; δ $P<0.05$  vs. RFLE-L). RFLE, *Rubus fruticosus* leaf extract; SO, sham operation; OP, operation; RFLE-L, operated and treated with low dose (30 mg/kg) of RFLE; RFLE-M, operated and treated with medium dose (60 mg/kg) of RFLE; RFLE-H, operated and treated with high dose (90 mg/kg) of RFLE; C-V, cresyl violet; Iba1, ionized calcium-binding adapter molecule 1; ROI, region of interest.



in the SO group ( $33.2 \pm 1.7$  vs.  $1.2 \pm 0.1$ ,  $P < 0.001$ ; Fig. 4A, C). However, the number of microglia was lower in the RFLE-L, -M, and -H groups than in the OP group significantly ( $P < 0.05$  and  $P < 0.01$ ) and dose-dependently ( $P < 0.05$  vs. RFLE-L). Collectively, these results suggest that RFLE uptake attenuates both VaD-associated neuronal loss and associated microglial activation.

### RFLE inhibits the production of inflammatory mediators in LPS-challenged microglia

To investigate the possible mechanisms underlying the RFLE-mediated attenuation of microglial activation, we designed an *in vitro* study using a murine microglial cell line, BV-2. First, the optimal concentrations for studying the modulatory effect of RFLE on BV-2 cells were determined by a cell viability assay in the presence or absence of LPS challenge. As shown in Fig. 5A, 6 hours of treatment of RFLE showed no cytotoxicity at any concentration (50–200  $\mu\text{g/ml}$ ), regardless of LPS challenge. Accordingly, we used RFLE at these concentrations for further studies focusing on the evaluation of the possible inhibitory effects on the production of proinflammatory mediators including NO, TNF- $\alpha$ , and IL-6

(Fig. 5B–D, respectively). In response to LPS, all of them were markedly elevated ( $P < 0.001$  vs. without LPS). However, when the cells were pretreated with the indicated concentrations of RFLE for 12 hours, the LPS-induced production of NO, TNF- $\alpha$ , and IL-6 significantly decreased ( $P < 0.05$ ,  $P < 0.01$ , and  $P < 0.001$ , respectively, vs. untreated cells). RFLE pretreatment did not affect the production of these proinflammatory mediators under LPS-free conditions. Together, these results indicate that RFLE suppressed the production of proinflammatory mediators in activated microglia.

### RFLE inhibits MAPKs/NF- $\kappa$ B/iNOS signaling in LPS-challenged microglia

It has been reported that activation of MAPKs and the NF- $\kappa$ B pathway acts as the key upstream proinflammatory mediators in various innate immune cells, including microglia [27]. Thus, we analyzed the phosphorylation dynamics of three kinds of MAPKs, that is, p38, ERK, and JNK, and the nuclear translocation of cytosolic NF- $\kappa$ B in RFLE-pretreated BV-2 cells upon LPS challenge. As observed in the blot images (Fig. 6A) and their quantification graphs (Fig. 6B, C for p38 and ERK1/2, respectively), pretreatment with

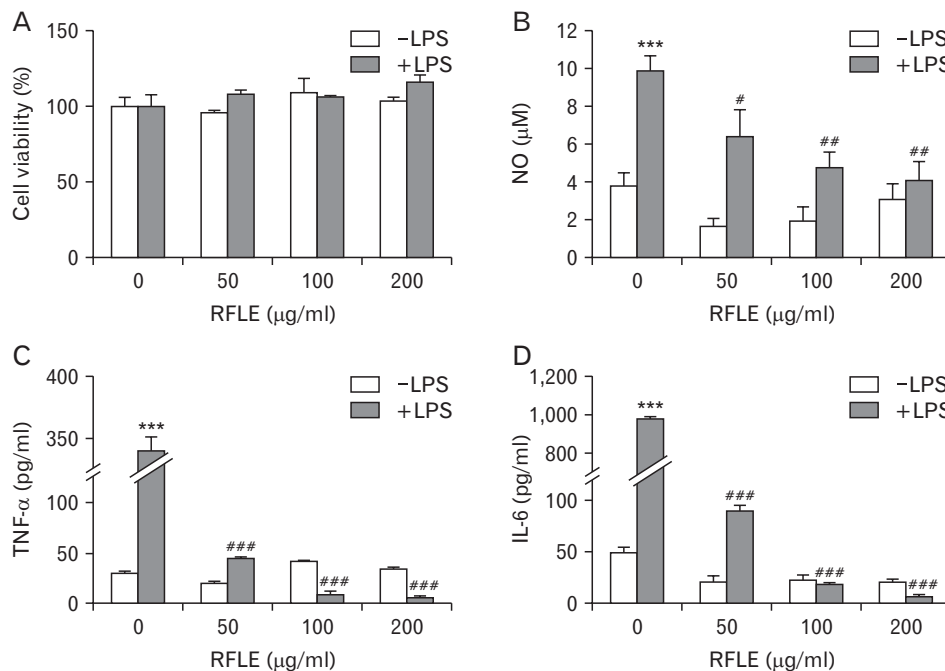


**Fig. 5.** Effect of RFLE on BV-2 microglial cell viability and lipopolysaccharide (LPS)-triggered production of pro-inflammatory mediators. BV-2 cells were pretreated with the indicated doses of RFLE for 6 hours and further treated with or without 1  $\mu\text{g/ml}$  LPS. After 18 hours, (A) cell viability and the released amounts of (B) nitric oxide, (C) TNF- $\alpha$ , and (D) IL-6 were evaluated. In all graphs, values are presented as mean  $\pm$  SEM ( $***P < 0.001$  vs. LPS-untreated control;  $\#P < 0.05$ ,  $##P < 0.01$ , and  $###P < 0.001$  vs. RFLE-untreated). RFLE, *Rubus fruticosus* leaf extract; NO, nitric oxide; TNF- $\alpha$ , tissue necrosis factor- $\alpha$ ; IL-6, interleukin-6.

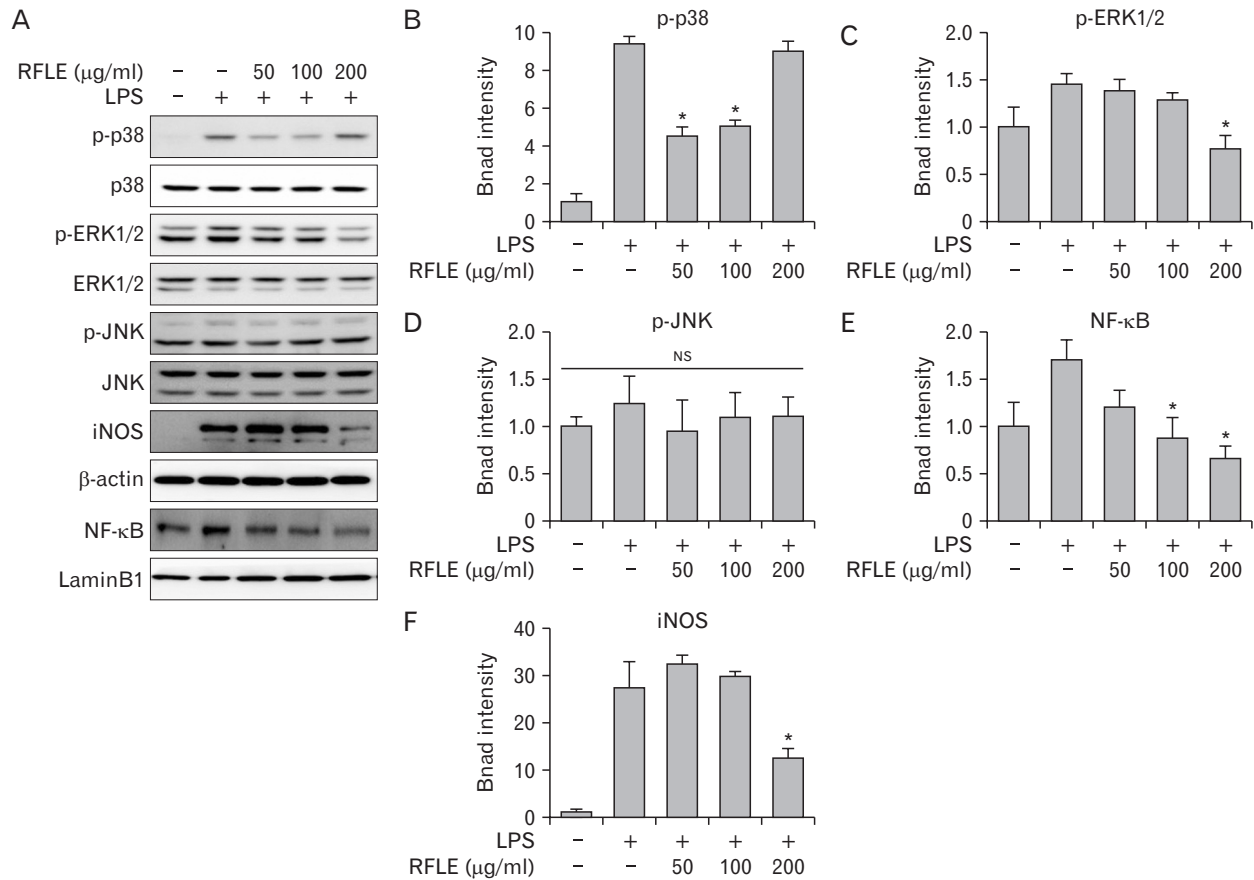


**Fig. 6.** Effect of RFLE on MAPK/NF-κB/iNOS signaling pathways in lipopolysaccharide (LPS)-challenged BV-2 cells. BV-2 cells were pretreated with the different dose of RFLE for 6 hours and further treated with 1 μg/ml LPS for 18 hours. (A) Representative western band images and (B–F) the quantitative graphs of p-p38, p-ERK1/2, p-JNK, nuclear NF-κB, and iNOS. The band intensities of p-p38, p-ERK1/2, p-JNK, and iNOS were normalized by β-actin. NF-κB intensity was normalized by laminB1, the internal controls. Data were expressed as fold of the controls (RFLE- and LPS-untreated) and collected from at least three independent experiments. Values are presented as mean±SEM (\**P*<0.05 vs. RFLE-untreated and LPS-treated). RFLE, *Rubus fruticosus* leaf extract; MAPK, mitogen-activated protein kinase; NF-κB, nuclear factor kappa B; iNOS, inducible nitric oxide synthase; ERK, extracellular signal-regulated kinase; JNK, c-Jun N-terminal kinase; NS, not significant.

specific concentrations of RFLE significantly suppressed the LPS-induced phosphorylation of p38 and ERK1/2 (*P*<0.05 vs. LPS only; 50 and 100 μg/ml for p-p38 and 200 μg/ml for p-ERK1/2), except for phosphorylation status of JNK (not significant throughout entire cell groups; Fig. 6A, D). Furthermore, LPS-induced nuclear translocation of NF-κB was significantly inhibited by pretreatment with RFLE (*P*<0.05 vs. LPS only; Fig. 6A, E). The expression of iNOS, the downstream of MAPK and NF-κB, was intensely induced by LPS challenge; however, pretreatment with 200 μg/ml RFLE significantly suppressed this level (*P*<0.05 vs. LPS only; Figs. 6A, F). Together, these results have shown that downregulation of MAPKs/NF-κB/iNOS pathway is attributable to the RFLE-mediated attenuation of NO, TNF-α, and IL-6 release

in activated microglia.

### Discussion

In the present study, we investigated whether RFLE could exert a therapeutic role against VaD. Using an *in vivo* model of VaD, we demonstrated that RFLE could protect against VaD-induced memory deficits and hippocampal neuronal death, and microgliosis. Furthermore, using LPS-induced microglial activation *in vitro*, we showed that RFLE could inhibit the production of proinflammatory mediators such as NO, TNF-α, and IL-6, and key upstream signaling pathways, such as MAPKs and NF-κB.

VaD is a neurodegenerative disorder accompanied by de-

terioration in memory function as a consequence of cerebrovascular accidents [2, 28]. The VaD pathogenesis has been known to be complex and multifaceted, mainly involving oxidative stress, neuronal apoptosis, and imbalance of tone of excitatory and inhibitory neurotransmitters [29]. Remarkably, a body of evidence has shown that neuroinflammation is essentially associated with memory impairment in VaD [30, 31]. During the neuroinflammatory process, microglia are activated and produce proinflammatory mediators that directly affect neuronal function, such as long-term potentiation, glutamate release, glutamate receptor trafficking, and activation of cell signaling pathways, which are related to synaptic plasticity and neurotransmission [32]. These changes converge on the impairment of neuronal processes related to cognition [7, 33]. Furthermore, the released proinflammatory mediators favor dysfunction of the blood-brain barrier, and subsequent extravasation of peripheral leukocytes occurs in the CNS [5, 34]. These phenomena can further exaggerate neuroinflammation. Accordingly, the development of new therapeutics that can counteract microglial activation is urgently needed.

Owing to the desire for nontoxic and brain-deliverable therapeutic candidates, there has been a growing interest in the promising effects of agricultural products on neurodegenerative diseases in recent years [35]. A large number of experimental and epidemiological studies strongly support this expectation by unveiling active phenolic substances with potent antioxidative and anti-inflammatory properties contained in some of those products [36]. Among polyphenols, EA stands out, which is relatively stable under physiological conditions in the stomach and can be a potential phytotherapeutic candidate for the development of neuroprotective drugs that can be administered orally [21, 37]. EA has multiple pharmacological properties that are useful in the treatment and maintenance of CNS disorders. It can regulate several molecular signaling pathways to normalize mitochondrial dysfunction that results in the generation of free radicals and thus attenuate neurodegeneration [37, 38]. The antioxidant action of EA is because of its ability to scavenge free radicals and potentiate endogenous antioxidants. EA can protect the brain from inflammation by downregulating the expression of several proinflammatory cytokines [39]. A previous study showed that EA could reduce the release of proinflammatory cytokines from microglia and the accumulation of amyloid plaques in an AD animal model [40]. In this study, we confirmed by HPLC that RFLE contains EA as

a major polyphenolic compound.

When considering a body of evidence regarding the well-known neuroprotective effects of EA as introduced earlier, it is reasonable that RFLE, as a rich source of this polyphenol, may be also neuroprotective. However, to the best of our knowledge, there has been no study on the anti-VaD potential of RFLE to date. This is due, at least in part, to the lack of unified and reproducible methods for establishing rodent VaD models [41]. At present, BCCAO (also named 2-vessel occlusion) in rats is the most commonly utilized rodent VaD model [25]. However, incomplete interruption of CBF via the patent vertebral arteries (VA) and the resulting inadequate and slow development of dementia phenotypes limits their widespread use as an experimental platform for drug screening [25, 42]. In contrast to the issue surrounding BCCAO, transient BCCAO combined with bilateral VA occlusion (also named 4-vessel occlusion), another popular modeling technique for VaD, is reported to be highly invasive and lethal, further increasing the number of rats required [25]. To overcome the major drawbacks of 2- and 4-vessel occlusion techniques, we utilized BCCAO/H, a relatively new technique for generating the VaD model [25, 43]. We confirmed that this technique produced a reproducible injury to the hippocampus without a high mortality rate in several preliminary trials. The reliability of this model is attributed to the real-time monitoring of rCBF dynamics during the ischemic period. An 8-minute period of ischemic insult produced selective damage to the hippocampus, while less vulnerable brain regions were unaffected, thus yielding functional defects of hippocampus-dependent memory without prefrontal cortex-dependent affective or motor, as supported by this study (Fig. 3E, G).

This study, for the first time, provided evidence of the anti-VaD effects of RFLE, showing the attenuation of memory deficits and neuronal death in the hippocampus, two representative findings of VaD. By performing an *in vitro* experiment, we demonstrated that these effects are attributable to the attenuation of microglial activation. In BV-2 cells challenged with LPS, all three types of MAPK were phosphorylated. However, RFLE inhibited the phosphorylation of p38 and ERK1/2, but not JNK. Surprisingly, western blot data showed a bimodal pattern for p38 phosphorylation, with increased phosphorylation after high-dose RFLE (200 µg/ml) treatment (Fig. 5A, B). To confirm the effect of RFLE on p38 phosphorylation, it is necessary to verify the specificity of the antibodies and validate the experimental conditions, such as

treatment time.

This study still has some limitations. First, in this study, RFLE was administered five times, but it was sequentially taken in the preoperative and PODs. Thus, we could not elucidate whether RFLE intake is therapeutic, that is, it may be useful after VaD occurs, or preventive. To give salvation to this issue, further studies using binary protocols, such as pretreatment versus posttreatment, are needed. Second, this study had shortcomings in detailed explanations of the major mechanisms underlying RFLE-induced anti-VaD effects *in vivo*. Although the possible modulation of microglial activation by RFLE was the main focus of this study, we cannot rule out the possibility that RFLE has a modulatory role on other cellular components in the CNS. As such, recent studies emphasize that research on the pathogenesis of many CNS disorders and their therapeutic modalities should consider multicellular dysfunction within the CNS microenvironment [43]. The neurogliovascular unit, which is a structurally and functionally interconnected network of neurons, glial cells (microglia and astrocytes), and vascular cells (*e.g.*, endothelial cells), has emerged as the basic element providing a framework of the CNS [44]. VaD involves a complicated pathogenesis, including a complex mixture of cellular and molecular events besides neuroinflammation, including neuronal apoptosis [45], impaired neurogenesis [46], dysfunctional blood-brain barrier [47], and altered glymphatic system [48]. In line with these notions, more advanced, well-designed, and multicellular approaches should be furtherly executed to reveal the specific mode of action of the RFLE on VaD.

## ORCID

Nak Song Sung: <https://orcid.org/0000-0002-7549-3829>  
 Sun Ho Uhm: <https://orcid.org/0009-0007-5053-5766>  
 Hyun Bae Kang: <https://orcid.org/0000-0002-1203-8618>  
 Nam Seob Lee: <https://orcid.org/0000-0001-6817-5403>  
 Young-Gil Jeong: <https://orcid.org/0000-0001-8696-107X>  
 Do Kyung Kim: <https://orcid.org/0000-0001-6655-7061>  
 Nak-Yun Sung: <https://orcid.org/0000-0002-7506-8697>  
 Dong-Sub Kim: <https://orcid.org/0000-0002-6843-0360>  
 Young Choon Yoo: <https://orcid.org/0000-0001-8905-6104>  
 Seung Yun Han: <https://orcid.org/0000-0002-7055-6341>

## Author Contributions

Conceptualization: NSS, SYH, NYS. Data acquisition: SHU, HBK, DSK. Data analysis or interpretation: NSL, YGJ, DKK, YCY. Drafting of the manuscript: NSS, SYH. Critical revision of the manuscript: SHU, HBK, SYH. Approval of the final version of the manuscript: all authors.

## Conflicts of Interest

No potential conflict of interest relevant to this article was reported.

## Funding

This work was supported by Konyang University Myung-gok Research Fund (2018) and Basic Research Program funded by Ministry of Science and ICT (RS-2023-00251456).

## References

1. Plassman BL, Langa KM, Fisher GG, Heeringa SG, Weir DR, Ofstedal MB, Burke JR, Hurd MD, Potter GG, Rodgers WL, Steffens DC, Willis RJ, Wallace RB. Prevalence of dementia in the United States: the aging, demographics, and memory study. *Neuroepidemiology* 2007;29:125-32.
2. Bastos-Leite AJ, van der Flier WM, van Straaten EC, Staekenborg SS, Scheltens P, Barkhof F. The contribution of medial temporal lobe atrophy and vascular pathology to cognitive impairment in vascular dementia. *Stroke* 2007;38:3182-5.
3. Sun M, Shen X, Ma Y. Rehmannioside A attenuates cognitive deficits in rats with vascular dementia (VD) through suppressing oxidative stress, inflammation and apoptosis. *Biomed Pharmacother* 2019;120:109492.
4. Luo XQ, Li A, Yang X, Xiao X, Hu R, Wang TW, Dou XY, Yang DJ, Dong Z. Paeoniflorin exerts neuroprotective effects by modulating the M1/M2 subset polarization of microglia/macrophages in the hippocampal CA1 region of vascular dementia rats via cannabinoid receptor 2. *Chin Med* 2018;13:14.
5. Stanimirovic D, Satoh K. Inflammatory mediators of cerebral endothelium: a role in ischemic brain inflammation. *Brain Pathol* 2000;10:113-26.
6. Ueno M. [Elucidation of mechanism of blood-brain barrier damage for prevention and treatment of vascular dementia]. *Rinsho Shinkeigaku* 2017;57:95-109. Japanese.
7. Cechetti F, Pagnussat AS, Worm PV, Elsner VR, Ben J, da Costa MS, Mestriner R, Weis SN, Netto CA. Chronic brain hypoperfusion causes early glial activation and neuronal death, and subsequent long-term memory impairment. *Brain Res Bull* 2012;87:109-16.

8. Sinha K, Sun C, Kamari R, Bettermann K. Current status and future prospects of pathophysiology-based neuroprotective drugs for the treatment of vascular dementia. *Drug Discov Today* 2020;25:793-9.
9. Daglia M. Polyphenols as antimicrobial agents. *Curr Opin Biotechnol* 2012;23:174-81.
10. Xie Y, Chen J, Xiao A, Liu L. Antibacterial activity of polyphenols: structure-activity relationship and influence of hyperglycemic condition. *Molecules* 2017;22:1913.
11. Mhatre S, Srivastava T, Naik S, Patravale V. Antiviral activity of green tea and black tea polyphenols in prophylaxis and treatment of COVID-19: a review. *Phytomedicine* 2021;85:153286.
12. Luo J, Si H, Jia Z, Liu D. Dietary anti-aging polyphenols and potential mechanisms. *Antioxidants (Basel)* 2021;10:283.
13. Korkina LG, De Luca C, Kostyuk VA, Pastore S. Plant polyphenols and tumors: from mechanisms to therapies, prevention, and protection against toxicity of anti-cancer treatments. *Curr Med Chem* 2009;16:3943-65.
14. Yang CS, Lambert JD, Sang S. Antioxidative and anti-carcinogenic activities of tea polyphenols. *Arch Toxicol* 2009;83:11-21.
15. Yahfoufi N, Alsadi N, Jambi M, Matar C. The immunomodulatory and anti-inflammatory role of polyphenols. *Nutrients* 2018;10:1618.
16. Zia-Ul-Haq M, Riaz M, De Feo V, Jaafar HZ, Moga M. *Rubus fruticosus* L.: constituents, biological activities and health related uses. *Molecules* 2014;19:10998-1029.
17. Zafra-Rojas QY, González-Martínez BE, Cruz-Cansino NDS, López-Cabanillas M, Suárez-Jacobo Á, Cervantes-Elizarrarás A, Ramírez-Moreno E. Effect of ultrasound on *in vitro* bioaccessibility of phenolic compounds and antioxidant capacity of blackberry (*Rubus fruticosus*) residues cv. Tupy. *Plant Foods Hum Nutr* 2020;75:608-13.
18. Verma R, Gangrade T, Punasiya R, Ghulaxe C. *Rubus fruticosus* (blackberry) use as an herbal medicine. *Pharmacogn Rev* 2014;8:101-4.
19. Weli AM, Al-Saadi HS, Al-Fudhaili RS, Hossain A, Putit ZB, Jasim MK. Cytotoxic and antimicrobial potential of different leaves extracts of *R. fruticosus* used traditionally to treat diabetes. *Toxicol Rep* 2020;7:183-7.
20. Dou ZM, Chen C, Huang Q, Fu X. The structure, conformation, and hypoglycemic activity of a novel heteropolysaccharide from the blackberry fruit. *Food Funct* 2021;12:5451-64.
21. Gudej J, Tomczyk M. Determination of flavonoids, tannins and ellagic acid in leaves from *Rubus* L. species. *Arch Pharm Res* 2004;27:1114-9.
22. Riaz M, Zia-Ul-Haq M, Ur-Rahman N, Ahmadi M. Neuropharmacological effects of methanolic extracts of *Rubus fruticosus* L. *Turk J Med Sci* 2014;44:454-60.
23. Carbone L. Pain management standards in the eighth edition of the Guide for the Care and Use of Laboratory Animals. *J Am Assoc Lab Anim Sci* 2012;51:322-8.
24. Nair AB, Jacob S. A simple practice guide for dose conversion between animals and human. *J Basic Clin Pharm* 2016;7:27-31.
25. Sanderson TH, Wider JM. 2-vessel occlusion/hypotension: a rat model of global brain ischemia. *J Vis Exp* 2013;76:50173.
26. Kang HB, Kim SH, Uhm SH, Kim DK, Lee NS, Jeong YG, Sung NY, Kim DS, Han IJ, Yoo YC, Han SY. *Perilla frutescens* leaf extract attenuates vascular dementia-associated memory deficits, neuronal damages, and microglial activation. *Curr Issues Mol Biol* 2022;44:257-72.
27. Olsson B, Hertz J, Lautner R, Zetterberg H, Nägga K, Höglund K, Basun H, Annas P, Lannfelt L, Andreassen N, Minthon L, Blennow K, Hansson O. Microglial markers are elevated in the prodromal phase of Alzheimer's disease and vascular dementia. *J Alzheimers Dis* 2013;33:45-53.
28. Fitzpatrick AL, Kuller LH, Lopez OL, Kawas CH, Jagust W. Survival following dementia onset: Alzheimer's disease and vascular dementia. *J Neurol Sci* 2005;229-30:43-9.
29. Wang J, Zhang HY, Tang XC. Cholinergic deficiency involved in vascular dementia: possible mechanism and strategy of treatment. *Acta Pharmacol Sin* 2009;30:879-88.
30. Lyman M, Lloyd DG, Ji X, Vizcaychipi MP, Ma D. Neuroinflammation: the role and consequences. *Neurosci Res* 2014;79:1-12.
31. Chen WW, Zhang X, Huang WJ. Role of neuroinflammation in neurodegenerative diseases (Review). *Mol Med Rep* 2016;13:3391-6.
32. Riazi K, Galic MA, Kentner AC, Reid AY, Sharkey KA, Pittman QJ. Microglia-dependent alteration of glutamatergic synaptic transmission and plasticity in the hippocampus during peripheral inflammation. *J Neurosci* 2015;35:4942-52.
33. Damodaran T, Müller CP, Hassan Z. Chronic cerebral hypoperfusion-induced memory impairment and hippocampal long-term potentiation deficits are improved by cholinergic stimulation in rats. *Pharmacol Rep* 2019;71:443-8.
34. Muldoon LL, Alvarez JI, Begley DJ, Boado RJ, Del Zoppo GJ, Doolittle ND, Engelhardt B, Hallenbeck JM, Lonser RR, Ohlfest JR, Prat A, Scarpa M, Smeyne RJ, Drewes LR, Neuwelt EA. Immunologic privilege in the central nervous system and the blood-brain barrier. *J Cereb Blood Flow Metab* 2013;33:13-21.
35. Solanki I, Parihar P, Parihar MS. Neurodegenerative diseases: from available treatments to prospective herbal therapy. *Neurochem Int* 2016;95:100-8.
36. Bhullar KS, Rupasinghe HP. Polyphenols: multipotent therapeutic agents in neurodegenerative diseases. *Oxid Med Cell Longev* 2013;2013:891748.
37. Ahmed T, Setzer WN, Nabavi SF, Orhan IE, Braidy N, Sobarzo-Sanchez E, Nabavi SM. Insights into effects of ellagic acid on the nervous system: a mini review. *Curr Pharm Des* 2016;22:1350-60.
38. Wei YZ, Zhu GF, Zheng CQ, Li JJ, Sheng S, Li DD, Wang GQ, Zhang F. Ellagic acid protects dopamine neurons from rotenone-induced neurotoxicity via activation of Nrf2 signalling. *J Cell Mol Med* 2020;24:9446-56.
39. Chen P, Chen F, Zhou B. Antioxidative, anti-inflammatory and anti-apoptotic effects of ellagic acid in liver and brain of rats treated by D-galactose. *Sci Rep* 2018;8:1465. Erratum in: *Sci*

- Rep 2019;9:19129.
40. Jha AB, Panchal SS, Shah A. Ellagic acid: insights into its neuroprotective and cognitive enhancement effects in sporadic Alzheimer's disease. *Pharmacol Biochem Behav* 2018;175:33-46.
  41. Macrae IM. Preclinical stroke research--advantages and disadvantages of the most common rodent models of focal ischaemia. *Br J Pharmacol* 2011;164:1062-78.
  42. León-Moreno LC, Castañeda-Arellano R, Rivas-Carrillo JD, Dueñas-Jiménez SH. Challenges and improvements of developing an ischemia mouse model through bilateral common carotid artery occlusion. *J Stroke Cerebrovasc Dis* 2020;29:104773.
  43. Burda JE, Sofroniew MV. Reactive gliosis and the multicellular response to CNS damage and disease. *Neuron* 2014;81:229-48.
  44. Zhang JH, Badaut J, Tang J, Obenaus A, Hartman R, Pearce WJ. The vascular neural network--a new paradigm in stroke pathophysiology. *Nat Rev Neurol* 2012;8:711-6.
  45. Zhang LM, Jiang CX, Liu DW. Hydrogen sulfide attenuates neuronal injury induced by vascular dementia via inhibiting apoptosis in rats. *Neurochem Res* 2009;34:1984-92.
  46. Kwon KJ, Kim MK, Lee EJ, Kim JN, Choi BR, Kim SY, Cho KS, Han JS, Kim HY, Shin CY, Han SH. Effects of donepezil, an acetylcholinesterase inhibitor, on neurogenesis in a rat model of vascular dementia. *J Neurol Sci* 2014;347:66-77.
  47. Bhatia P, Singh N. Tadalafil ameliorates memory deficits, oxidative stress, endothelial dysfunction and neuropathological changes in rat model of hyperhomocysteinemia induced vascular dementia. *Int J Neurosci* 2022;132:384-96.
  48. Venkat P, Chopp M, Zacharek A, Cui C, Zhang L, Li Q, Lu M, Zhang T, Liu A, Chen J. White matter damage and glymphatic dysfunction in a model of vascular dementia in rats with no prior vascular pathologies. *Neurobiol Aging* 2017;50:96-106.